UJEAS

UNIZIK JOURNAL OF ENGINEERING AND APPLIED SCIENCES

UNIZIK Journal of Engineering and Applied Sciences 6(3), September (2026), 3726-3742
Journal homepage: https://journals.unizik.edu.ng/index.php/ujeas
PRINT ISSN: 2992-4383 || ONLINE ISSN: 2992-4391

Synthesis of Cellulose Based Carbon Dots from African fan palm (Borassus aethiopum) for Corrosion Inhibition of Mild Steel in HCL

Izuchukwu O. Madu*
Department of Polymer Engineering, Nnamdi Azikiwe University, Awka, Nigeria
Joseph T. Nwabanne
Department of Chemical Engineering, Nnamdi Azikiwe University, Awka, Nigeria
Iheoma C. Nwuzor
Department of Polymer Engineering, Nnamdi Azikiwe University, Awka, Nigeria
Victor U. Okpechi
Department of Polymer Engineering, Nnamdi Azikiwe University, Awka, Nigeria

Corresponding Author's E-mail: io.madu@unizik.edu.ng

Abstract
This study investigated the synthesis of lignin-containing cellulose carbon dots (LC-CDs) from African fan palm (*Borassus aethiopum*) biomass and their application as eco-friendly corrosion inhibitors for mild steel in 1 M HCl solution. The cellulose-rich fibres were treated with alkali and converted into carbon dots through hydrothermal synthesis. The prepared LC-CDs were characterized using UV–Visible spectroscopy, Fourier Transform Infrared Spectroscopy (FTIR), Transmission Electron Microscopy (TEM), and Scanning Probe Microscopy (SPM). Results confirmed the successful formation of spherical carbon dots with particle sizes below 10 nm and abundant oxygen-containing functional groups. Corrosion inhibition performance was evaluated using weight loss analysis, electrochemical impedance spectroscopy (EIS), potentiodynamic polarization (PDP), scanning electron microscopy (SEM), energy dispersive spectroscopy (EDS), and atomic force microscopy (AFM). The inhibition efficiency increased with concentration and immersion time, reaching optimum efficiencies of 90.8% and 90.7% from weight loss and electrochemical measurements, respectively, at 200 mg/L. Electrochemical studies showed reduced corrosion current density and increased charge transfer resistance, indicating effective adsorption and protective film formation on the steel surface. The results demonstrate that African fan palm-derived LC-CDs are sustainable, low-cost, and highly effective green corrosion inhibitors for acidic industrial environments.

Keywords: Carbon dots, Lignin containing cellulose, synthesis, Borassus aethiopum, corrosion inhibition, mild steel.

1. Introduction

In many modern industries, metal materials play a crucial role. At the same time, metal corrosion is common and causes very serious damage (Bender et al., 2022; Zehra et al., 2025). The damage that metals and alloys sustain from chemical or electrochemical interactions with their surroundings is known as corrosion. Wet and dry corrosion are two categories of corrosion responses based on the types of corrosive conditions. General corrosion, pitting corrosion, crevice corrosion, intergranular corrosion, environmentally induced fracture, de-alloying, galvanic, and erosion-corrosion can all be categorized based on the morphology of metal degradation (Afolabi et al., 2024; Gitzhofer et al., 2021; Kadhim et al., 2021). Metal can be protected from corrosion in a number of ways, including coating, alloying, cathodic protection, anodic protection, and, more recently, laser surface treatment, which is thought to enhance the metal's hardness, roughness, corrosion resistance, and other qualities. Because they are widely used to reduce metallic waste during production and lower the danger of material failure both of which can result in the abrupt shutdown of industrial processes, which in turn results in higher costs. corrosion inhibitors are of significant practical value. Corrosion inhibitors are also crucial for preventing mineral dissolution and lowering acid usage (Avdeev & Kuznetsov, 2022).

One popular anti-corrosion technique is the addition of corrosion inhibitor, which has the advantages of being easy to use, inexpensive, and highly practical. A material that is introduced to a corrosive solution in modest amounts to slow down the pace of corrosion is called an inhibitor (Verma et al., 2021). This action is explained by the inhibitor particles adhering to the metal surface and forming a cohesive protective layer. It can prolong the equipment's service life and drastically lower the pace at which metal materials corrode. Certain conventional high-efficiency corrosion inhibitors, like chromate, phosphorus-containing compounds, and mercury salts, are poisonous and difficult to biodegrade. Therefore, in order to replace these conventional corrosion inhibitors, new environmentally friendly ones must be developed (Hossain et al., 2021). As of right now, corrosion inhibitors can be divided into two groups according to their chemical makeup: organic and inorganic. Nitrates, chromates, and

phosphates are examples of inorganic inhibitors that have demonstrated encouraging inhibiting activity. However, they don't adhere to environmental protection regulations because of their dangerous consequences. A number of organic inhibitors, such as amines and alkanol amines (Loachamin et al., 2024), amino acids (Al-Amiery et al., 2023), silanes (Al-Saadi & Singh Raman, 2022), ionic liquids (Ul Haq et al., 2022), and plant extracts (Holla et al., 2024; Li et al., 2025), have been developed to solve this problem. Due to their eco-friendliness, plant extracts and amino acids have been identified as green corrosion inhibitors, garnering increasing attention.

In addition to being biodegradable, green corrosion inhibitors are free of hazardous substances and heavy metals. Over time, there has been an increase in the search for naturally occurring organic compounds or biodegradable organic materials to utilize as corrosion inhibitors. There are numerous reports on the different natural compounds that are employed as green inhibitors. It has been noted that low-grade gram flour (Ahmed et al., 2024), natural honey (Vashi, 2025), onion (Galo et al., 2021), potato (Shekhar et al., 2021), gelatin (Kusumattaqiin et al., 2021), plant roots (Wang et al., 2023), leaves (Al Otaibi & Hammud, 2021), seeds (Shahmoradi et al., 2022), and floral gums (Vaidya et al., 2022) are effective inhibitors. These options do, however, still have certain disadvantages. In particular, the preparation of plant extracts frequently includes laborious processes and hazardous solvents, which might have an adverse effect on the environment. Amino acids are also not economical, which restricts their use. Therefore, it is imperative to create a simple, environmentally friendly process for creating a new, efficient green corrosion inhibitor.

Interestingly. Carbon dots (CDs) are an exciting option for the upcoming generation of green corrosion inhibitors since they are affordable, environmentally friendly, and simple to make. CDs are generally described as zero-dimensional carbon nanoparticles that are smaller than 10 nm and have fluorescence as an intrinsic characteristic (Abraham & Balachandran, 2022; Yadav & Daniel, 2024; Yang et al., 2023). CDs have been widely used thus far in a variety of sectors, including biology (Hui, 2023), sensing (MP et al., 2022), catalysis (Prakash et al., 2023), and lubrication (Kumar et al., 2022). Nevertheless, their use in the field of protecting against metal corrosion begins later. CDs were initially shown to be an effective corrosion inhibitor in 2017 (Dong et al., 2024). Carbon dots have been employed in anti-corrosion research because of their benefits, which include rich raw materials, good water solubility, non-pollution, low cost, and easy synthesis. Carbon dots (CDs) are luminous nanomaterials that lack dimensions. Carbon dots are currently a research hotspot because of their low toxicity, biocompatibility, and persistent fluorescence and chemical characteristics. CDs are useful in photocatalysis, biosensing, drug delivery, bioimaging, and other biological domains due to these exceptional qualities. Carbon dots have so far been produced by numerous researchers using hydrothermal (Nazibudin et al., 2023), (Kaczmarek et al., 2021), and microwave radiation (Karim et al., 2022). Spectrum range, fluorescence yield, and many other characteristics of CDs can be successfully improved by doping, especially when heteroatom doping is used (Tang et al., 2024).

Renewable raw materials are great prospects to serve as building blocks for novel compounds that prevent corrosion. They are rich in biomolecules with an abundance of C, N, O, S, and P, among other elements; they are inexpensive, abundant, natural, and can be obtained by the conversion of biomass (Gan et al., 2023). As an alternative to employing a residue or byproduct, using African fan palm (Borassus aethiopum) as a raw material to create CDs seems to be beneficial from an environmental perspective.

Borassus aethiopum, sometimes known as the African fan palm (AFP), is an evergreen palm tree with a single trunk and enormous fan-like leaves (Usman, 2025). In sub-Saharan Africa, AFP is a prominent and well-known feature of palm savannas. It develops a large stem that is around 20 to 25 meters tall and 80 to 85 centimeters in diameter. According to (Usman, 2025), the bluish-green fan-like leaves, including the petioles, can reach a maximum length of 3.5 meters, and the crown of AFP may be up to 8 meters broad. The regular burning and browsing of herbivores is ideal for Borassus aethiopumis. Borassus aethiopum is highly valued for sustenance by the local community in the locations where it is disseminated. The African fan palm's fruits, hypocotyls, boles, petioles, leaves, and blades are gathered for use in construction, medicine, and food. Fruits and young seedlings are consumed, and wine is tapped from the palm. Numerous human ailments are treated ethnomedically with the herb. The African fan palm's tree bowl, or stem, is used in construction and carpentry. The split leaves are used to weave domestic handicrafts, and the midribs are used to make brooms. Fibers that can be used as sponges can be obtained by soaking the ends of the leaf stalks in water. Fibers that can be used as filters or sponges can be obtained by soaking the ends of the leaf stalks in water. Extracts of *Borassus aethiopum* contain: Tannins, Flavonoids, Saponins, Alkaloids, Phenolic compounds with adsorption properties that makes it suitable for corrosion inhibition (Dave & Macwan, 2024). Carbon doting cellulose extract from Borassus aethiopum will not only improve the properties but preserve the inhibitor for better inhibitive performance in corrosion studies.

Several works have been reported by researchers on the use of carbon doting ecofriendly plant extracts for corrosion studies (Abd-El-Nabey et al., 2025; Cao et al., 2025; Xu et al., 2023). However, in this research work, cellulose, extracted from *African Fan Palm*, further synthesis in carbon dot to improve its efficiency for corrosion studies has not been previously studied except the one emanating from our laboratory. In this study, cellulose from the African fan palm (Borassus aethiopum) was used as a raw material to make carbon quantum dots. Because of its expanding potential and the industry's concerns about corrosion and the environment, its use as a corrosion

inhibitor for mild steel in 1 mol of HCl was evaluated. The study contributes to the growing field of green corrosion inhibitors by demonstrating that lignin-containing cellulose-based carbon dots (LC-CDs) can achieve high inhibition efficiency for mild steel in acidic environments while reducing reliance on toxic conventional inhibitors. This manuscript is important to the scientific community because it presents an environmentally sustainable approach for corrosion protection using biomass-derived carbon dots synthesized from African fan palm cellulose.

2.0 Materials and methods

2.1 Materials

Mature African fan palm (Borassus aethiopum) fruits were gathered from a plantation in Aniocha village, Ayamelum L. G. Area, Anambra state. Cellulose was prepared from the fibre using 2% sodium hydroxide solution. The carbon dot was synthesized and prepared from lignin containing cellulose derived from African fan palm (Borassus aethiopum) using Teflon-lined Hydrothermal autoclave. The mild steel specimens which were in form of strips were sourced from Bridge head, Onitsha metal's market Anambra state. The strips were subsequently subjected to elemental composition test using an optical emission spectroscopy (OES). Hydrochloric acid (Sigma Aldrich) and Ethanol (Scharlau) of analytical grades were used as solvent and reagents respectively.

A UV-Vis Spectrometer JASCO770, Tokyo, Japan was used to record the UV-visible absorption spectrum of the LC-CDs of 200 mg/l in aqueous solution. Using a KBr pellet and a Nicolet FTIR spectrometer (Impact-410, Madison, USA), the FTIR spectra of the LC-CDs was obtained. TEM images were recorded using a JEOL transmission electron microscope (JEM-2100F model) at an accelerating voltage of 200 kV. SPM image was obtained on a SPM, Dimension ICON, Bruker, Billerica, MA, United States.

2.2 Methods

2.2.1 Preparation of Lignin containing cellulose

In Aniocha village, Ayamelum L. G. Area, Anambra state, mature African fan palm (Borassus aethiopum) fruits were collected from a plantation. The fibers from these fruits were extracted by biological retting in stagnant water. The fruits were initially submerged in a basin of water at room temperature for seven days to allow the pectic components that connect the fibers to decompose. After being thoroughly cleaned several times, the fruits were left to air dry for five days. Using a knife, the fibrous cores were gently removed from the soft, flexible filaments. An electric grinder was used to crush the samples into a powder. The powdered materials were first mixed with a 2% sodium hydroxide solution and magnetically stirred for four hours at 80°C. After that, it was regularly washed with distilled water and dried in an air oven. This pulp was used to make lignocellulose (LC).

2.2.2 Chemical Composition

The chemical characterization was carried out at the Specialty and pulp limited, Ogun State. The following chemical analyses were performed in duplicate: carbohydrate content (glucans, xylans, galactans, mannans, and arabinans) lignin, uronic acids, hexenuronic acids, ash. The table shows the Analytical Procedures Used in Chemical Characterization

Carbohydrate content	SCAN-CM 71:09
Soluble lignin	GOLDSHIMID, 1971
Insoluble lignin	GOMIDE & DEMUNER, 1986
Uronic acids	SCOOT, 1979
Ash content	TAPPI 211 om-93

2.2.3 Preparation of biomass carbon dots

2 g of the lignin-containing cellulose (LC) was dispersed in 180 ml deionized water while stirring ultrasonically for 45 min to ensure their uniform dispersion. The mixtures were transferred to a 250 ml polytetrafluoroethylene hydrothermal autoclave and subjected to a temperature of 160^0C for 12 h. After the heating process, the solution was allowed to cool to room temperature and then filtered through a 0.22 μm microporous membrane to remove impurities. The filtered solutions were then transferred into a dialysis bag and the dialysis bag, containing the solution was placed in a beaker filled with ultra-pure water. The water in the beaker was replaced every 8 h, and this process was repeated three times. Following the completion of the dialysis process, the dialysate was collected and concentrated to 100 ml by a rotary evaporator. Finally, the concentrate was freeze-dried to obtain a powder of brown-black carbon dots which were stored in a desiccator for use.

2.2.4 Weight Loss Measurements

The mild steel strips were cut to measure 4 × 4 × 0.01 cm for the weight loss test and 1 cm2 for the electrochemical investigation. Different grades of silicon carbide sheets (220–1000 grit) were used to polish the mild steel strips. Before being used, the mild steel samples were thoroughly cleaned in ethanol and distilled water before being left to air dry. For mild steel weight loss tests at 30^0C, five distinct concentrations of the biomass carbon quantum dot (50, 100, 150, and 200mg) were produced in 1 M HCl. Initially, the mild steel samples were weighed, suspended in triplicate in 200 cm^3 of the test solution, and maintained in an aerated environment. The metal specimens were gradually removed from the test solutions for six days (144 hours). The mild steel was cleaned of corrosion products by immersing it in a Clark solution. The samples were then cleaned with distilled water and acetone, allowed to air dry, and then weighed once more using an analytical scale (precision = ±0.001 mg). Using the optimal concentration of the carbon dot under study, the experiment was repeated at 30, 40, 50, and 60°C at 24-hour intervals. The weight loss was calculated as the difference between the sample weights prior to and after immersion. The corrosion rates ($mmyr^{-1}$) and inhibition efficiency (IE) for weight loss measurements were calculated using equations 1 and 2 (Obot *et al.*, 2019) respectively:

$$\text{Corrosion rate (mm/yr)} = {87.6 \times 10^4 \times W}/{\rho \times A \times t} \quad (1)$$

where

W = Mild steel weight loss (g)

A = Mild steel exposed surface area (cm^2)

t = mild steel immersion time (h)

ρ = Mild steel density (7.86 g/cm^3)

The corrosion inhibition efficiency (IE %) shall be calculated using Equation 2

$$\text{IE\% (WL)} = {C_{R(blank)} - C_{R(inh)}}/{C_{R(blank)}} \quad (2)$$

Where:

$C_{R(blank)}$ = corrosion rate in the absence of the carbon dots (mm/yr)

$C_{R(inh)}$ = corrosion rate in the presences of the carbon dots (mm/yr)

3.0 Result and Discussion

Demuner (2017) describes the methods used to determine the chemical composition (acid-soluble lignin, acid-insoluble lignin, sugar composition, ash, uronic acid, hexenuronic acid), crystallinity index, maximal degradation temperature, and diameter of nanofibrils.

Table 1: Chemical composition of Lignin containing cellulose LC-CDs

Samples	Total lignin	Uronic acid	Hexenuronic	Ash	Glucan	Xylan	Mannnan	Galactan	Arabinan
LC	4.5	0.4	0.6	0.61	80.0	7.3	6.4	0.2	0.6

3.1 Characterization of LC-CDs and NLC-CDs

The structure of the as-prepared lignin-containing cellulose based carbon dots (LC-BCDs) was characterized using *Ultraviolet - Visible* spectroscopy (*UV - Vis)*, Fourier - Transform Infrared Spectroscopy (FTIR), and Transmission Electron Microscopy (TEM) techniques.

The Ultraviolet – Visible adsorption of the as-prepared lignin-containing cellulose based carbon dots (LC-CDs) was measured in the range of 200 – 500mm. The UV–vis absorption of the LC-CDs has characteristic peaks at 248 nm as shown in Fig. 1a. The peak at 248 nm was attributed to the π–π* electronic transition of conjugate structure of LC-CDs while the peak at 295 nm attributed to n-π* electronic transition of the C=O bonds of LC-CDs.

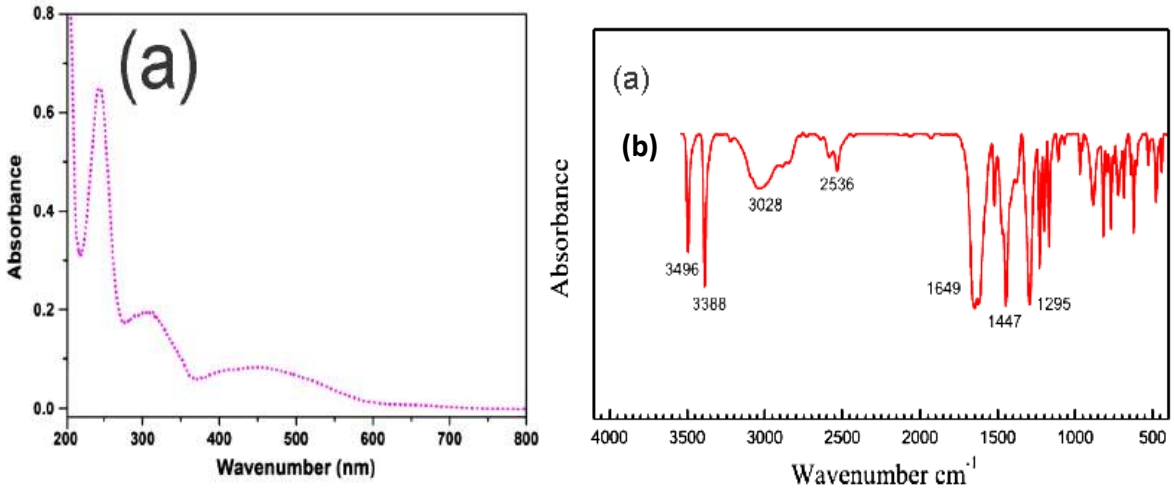

Figure 1: A) UV Spectra and B) FTIR curve for LC-CDs

Fourier Transform Infrared Spectroscopy (FTIR) technique was used to probe the functional groups present in LC-CDs. To obtain the characteristic adsorption bands of the LC-CDs, FT-IR measurements was carried out in the range of 500 – 4000 cm^{-1}, and the spectra are shown in Fig. 1b. Regarding to the spectrum of LC-CDs, the characteristic peaks are presented at 3362cm^{-1}, 2967 cm^{-1}, 2926 cm^{-1}, 1617 cm^{-1}, 1493 cm^{-1}, 1216 cm^{-1}, 810 cm^{-1}. The peak at 2926 LC-CDs is attributed to C-H stretching vibrations of LC-CDs

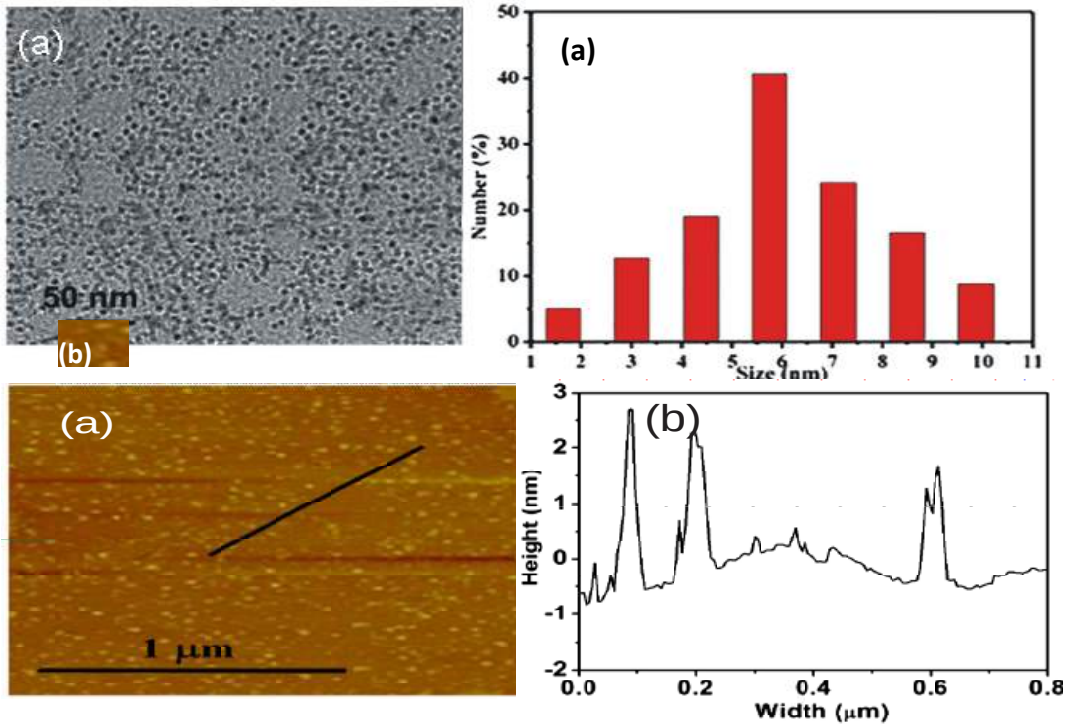

Figure 2: A) TEM micrograph for LC-CDs its corresponding Particles size distribution and B) SPM morphologies of LC-CDs and its corresponding Height profile line

Transmission electron microscopy was used to for the morphological and particle size characterization of LC-CDs. TEM images of LC-CDs are presented in Figure 2. As shown, the LC-CDs particles were of mainly spherical in shapes and evenly distributed, with the average particle size of 5.38nm. The obtained results indicated that carbon dots have been successfully formed, since their sizes were actually below less than 10 nm. The particle size and dispersion of the as-prepared LC-CDs were also examined using the scanning probe microscopy picture. LC-CDs

had a uniform dispersion without agglomeration and a grainy shape. According to statistics, the LC-CDs' height profiles were primarily dispersed between 6 and 12 nm, which is consistent with the TEM findings.

3.2 Studies on Corrosion Inhibition of Mild Steel in 1 M HCl

3.2.1 Weight Loss Measurements

The effectiveness of lignin-containing cellulose-based carbon dots (LC-CDs) as corrosion inhibitors rises with concentration up to 200 mg/L, as shown in Fig. 3(a–b). For example, Fig. 3(a–b) demonstrated that as the concentration of LC-CDs increased, the mild steel's corrosion rate in the 1 M HCl solution reduced. After 72 hours of immersion, the mild steel submerged in a 1 M HCl solution with 200 mg/L LC-CDs showed the lowest corrosion rate value of 2.37 mm/yr. This outcome demonstrated that LC-CDs have good corrosion inhibition. Additionally, Fig. 3(a–b) shows that the LC-CDs' inhibitory efficiency rise as their concentration rises to 200 mg. The mild steel submerged in a 1 M HCl solution with 200 mg/L LC-CDs had the maximum corrosion inhibition efficiency value of 90.8%. This outcome is consistent with how the concentration of inhibitors affects the rate of corrosion.

The impact of exposure time on mild steel corrosion behavior in a 1 M HCl solution with and without varying concentrations of cellulose-based carbon dots (LC-CDs) containing lignin was examined. The corrosion rate of mildly submerged 1 M HCl in the presence of any concentration of LC-CDs reduces with an extended immersion duration up to 72 hours, as shown in Fig. 3(a–b). Therefore, after 72 hours of immersion, the mild steel submerged in 1 M HCl solution containing 200 mg/L LC-CDs showed the lowest corrosion rate values, measuring 2.37 mm/yr.

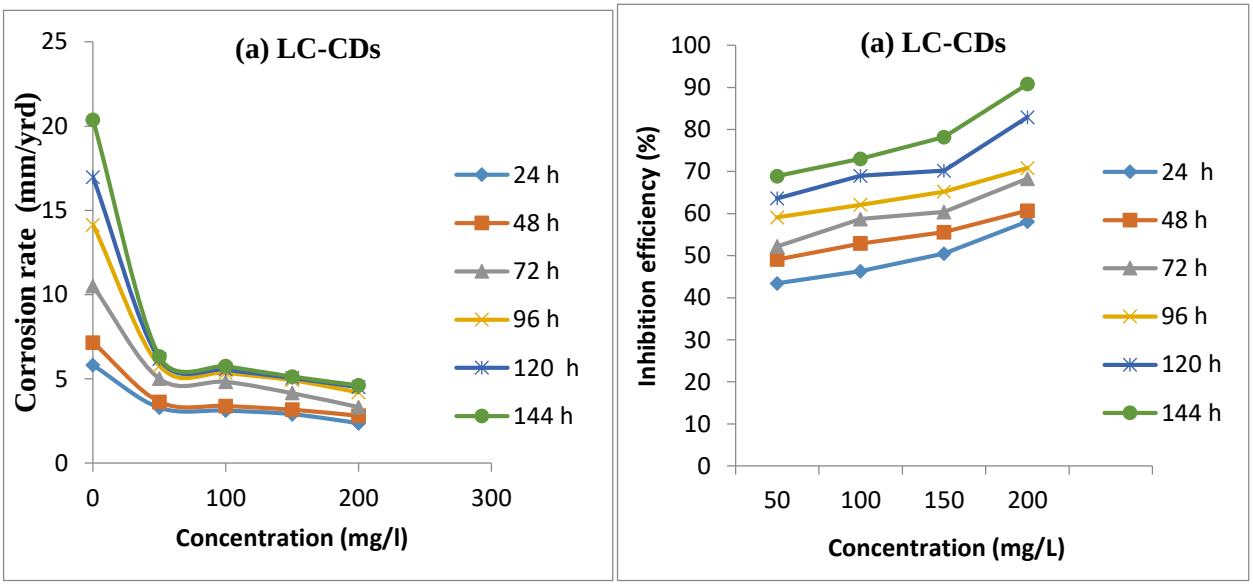

Figure 3 Effects of inhibitor concentration on A) corrosion rates and B) Inhibition efficiency of mild steel in 1 M HCl with LC-CDs at different immersion times at 25^{0}C

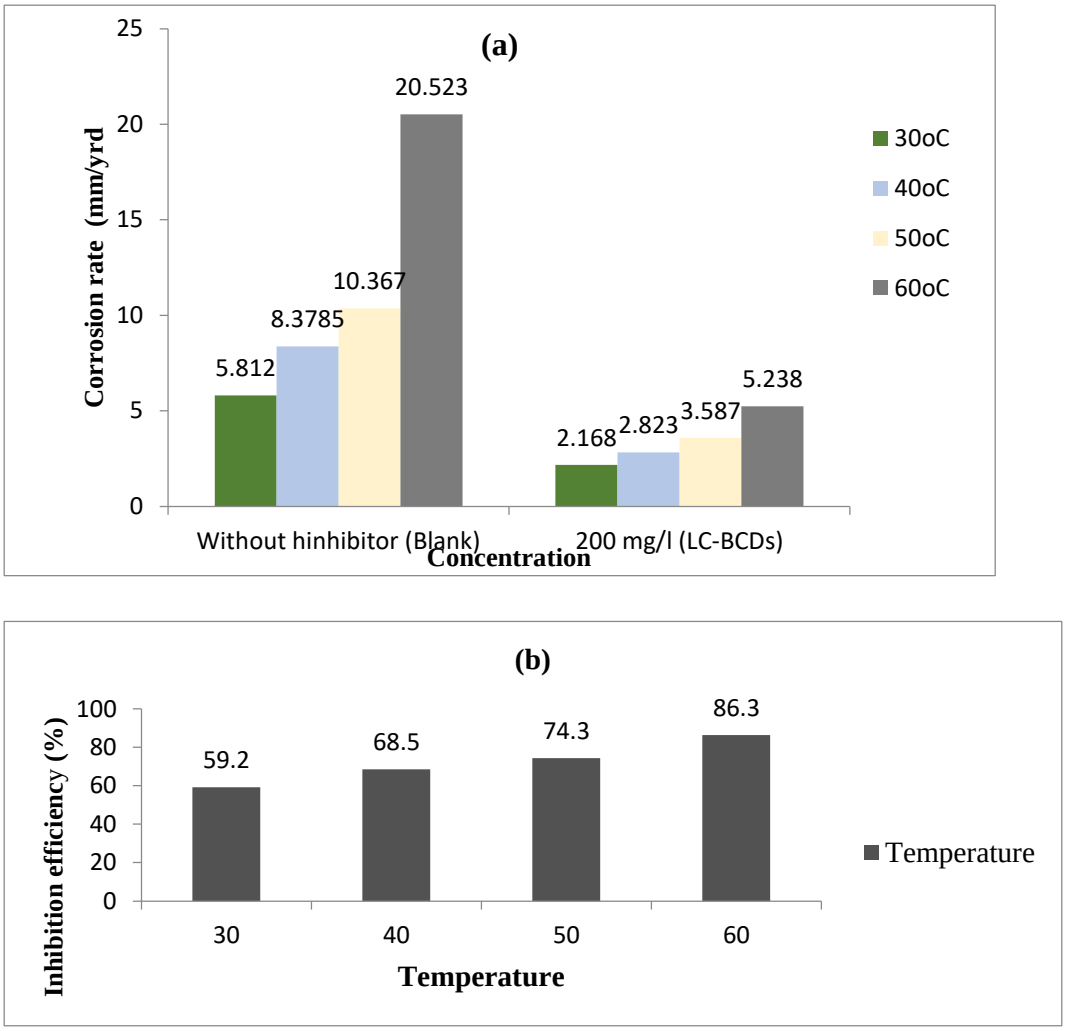

Figure 4. Variation of A) corrosion rates and B) Inhibition Efficiency of mild steel in 1 M HCl without, and with 200 mg/L of LC-CDs at different temperatures

After 24 hours, the corrosion rate in the blank solution was roughly 5.812 mm/yr at 30°C and considerably increased to 20.523 mm/yr at 60°C. However, the corrosion rate significantly decreased upon the addition of the LC-CDs. For example, the corrosion rate at 30 and 60 degrees Celsius was 2.3710 and 2.8116 mm/yr, respectively, when 200 mg/L LC-CDs were present. Figure 4 shows how LC-CDs corrosion inhibition efficiency changes with temperature at 200 mg/L after 24 hours. Figure 4b makes it evident that the efficiency of LC-CDs marginally increased with increasing temperature up 60^{o}C and this is a manifestation of chemisorption mechanism.

3.3 Adsorption Isotherm and Mechanism of Inhibition

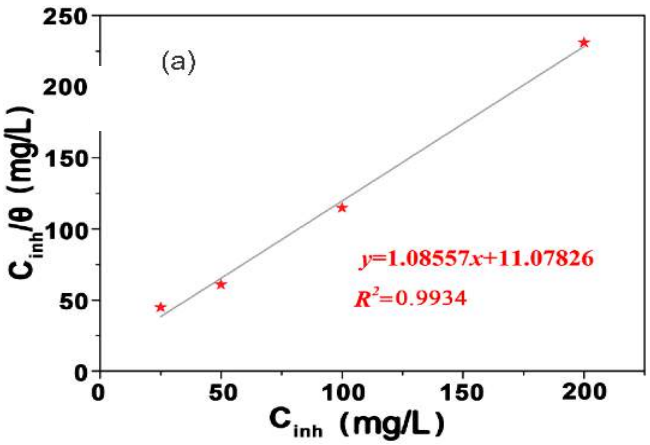

Figure 5: Linear Adsorption Plot of mild steel immersed in 1 M HCl solution in the presence of 200 mg/L LC-CDs 25^{0}C after 24 h.

Figure 5 is a linear adsorption plot commonly used in corrosion inhibition studies to analyze how an inhibitor adsorbs onto a metal surface.

with:

$$R^2 = 0.9934$$

indicates a very strong linear relationship.

This type of graph is characteristic of the Langmuir adsorption isotherm, which is expressed as:

$$\frac{C_{inh}}{\theta} = \frac{1}{K_{ads}} + C_{inh} \quad (3)$$

where:

- C_{inh}= inhibitor concentration
- θ= surface coverage
- K_{ads}= adsorption equilibrium constant

The near-unity slope (~1.09) and high R^2value suggest that the inhibitor adsorption follows the Langmuir adsorption model quite well. This implies: monolayer adsorption, homogeneous adsorption sites, minimal interaction between adsorbed molecules.

The result shows increasing inhibition efficiency with increasing temperature which is know to be Chemisorption. This indicates that the inhibitor remains effective under more aggressive conditions and are chemically adsorbing onto the metal surfaces. By spontaneously adsorbing oxygen-rich carbon dots onto the steel surface through electrostatic interactions and coordinate bonding between oxygen-containing functional groups and vacant iron d-orbitals, NLC-CDs inhibit mild steel corrosion in 1 M HCl. The adsorption process obeys the Langmuir isotherm (Figure 5) and produces a compact protective film that blocks active anodic and cathodic sites; the adsorbed layer suppresses iron dissolution, increases charge-transfer resistance, lowers double-layer capacitance, and minimizes surface deterioration. The observed temperature dependence and electrochemical parameters show that chemisorption predominates. This is supported by a research carried out by (Kellal et al., 2023), who disclosed several plant extracts with chemisorption adsorption mechanism due to their strong bong interaction between the inhibitor and the metal surface.

3.4 Electrochemical Measurements of Corrosion of Mild in 1 M HCl

Figures 6A show that the OCP curves grew more stable with increasing immersion time. Additionally, it was discovered that the addition of LC-CDs caused the open circuit potential to shift in the anodic direction, or toward higher values. As the concentration of LC-CDs increased, the value of OCP was observed to rise. Metal substrates are frequently less prone to corrosion when OCP levels are higher. Nonetheless, the difference in the OCP values of the mild steel sample in the blank and LC-CDs inhibited solutions was less than +85 mV vs Ag/AgCl for all LC-CD concentrations examined. A common classification for this sort of inhibitor is anodic-type inhibitors (Ituen et al., 2020; Ravi et al., 2023). Nyquist and related Bode graphs were examined using data from electrochemical impedance spectroscopy (EIS) measurements on the LC-CDs, Figures 6 display (A) OCP curves B) Nyquist, (C) Bode modulus, and (D) phase angle for LC-CDs.

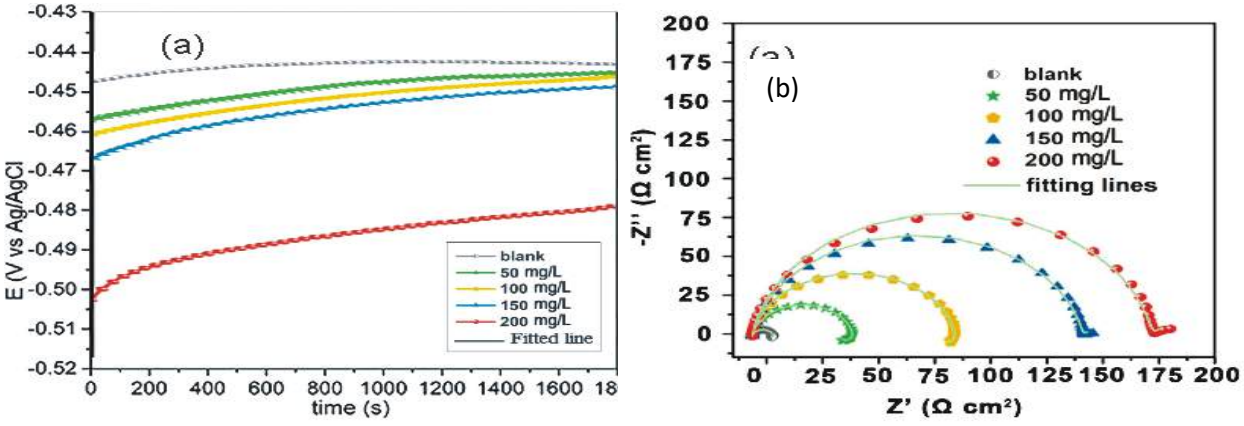

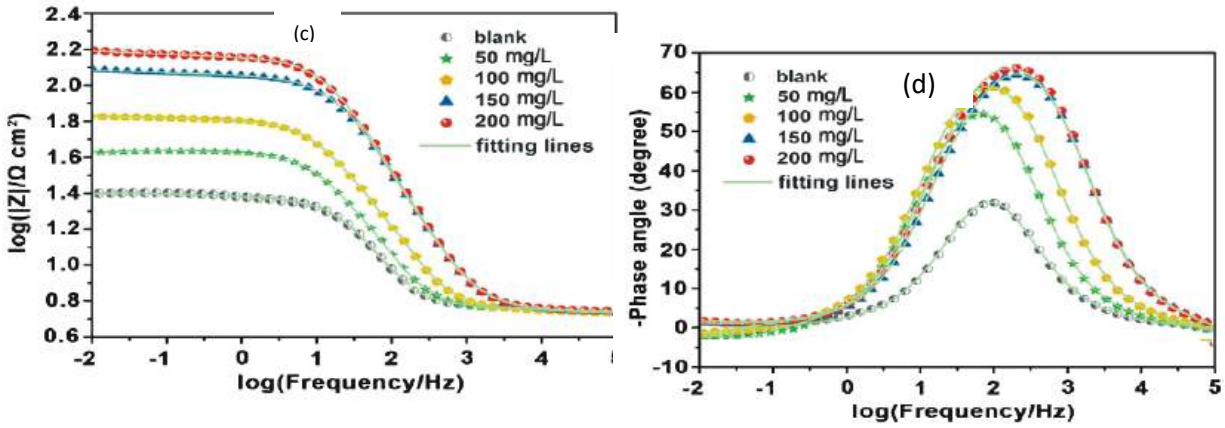

Figure 6: displays A) the time-dependent OCP curves B) Nyquist, (C) Bode modulus, and (D) phase angle of mild steel in 1 M HCl solution without and with LC-CDs at different concentrations.

Figure 6b displays the Nyquist plots of mild steel in 1 M HCl solutions with and without varying LC-CD concentrations. Regardless of whether LC-CDs were present or not, the Nyquist curves showed a same defective depressed capacitive loop. The Nyquist diagrams for systems including LC-CDs keep their shape but grow in size when compared to the blank. The arc's height and radius grow as the concentration of LC-CDs rises. This shows that without changing the charge transfer reaction mechanism, the addition of the corrosion inhibitor raises the impedance and prevents corrosion. The semicircle's size increases as the inhibitor concentration rises, most likely indicating a more potent inhibition when a greater composite concentration is used.

Additionally, Figure 6c shows Bode impedance modulus curves with and without varying LC-CD concentrations. The absolute impedance for mild steel in the acid solution with the

Table 2: Electrochemical parameters of LC-CDs

Conc. (mg/l)	R_s (Ω cm^2)	CPE_{dl}		R_{ct} (Ω cm^2)	CPE_f		R_f (Ω cm^2)	$R_p = (R_f + R_{ct})$ (Ω cm^2)	C_{dl} (μFcm^{-2})	x^2 ($\times10^{-3}$)	% IE
		Y_{dl} (μFcm^{-2} s^{n-1})(	n_{dl}		Y_f F cm^{-2} s^{n-1}) ($\times10^{-3}$)	n_f					
Blank	2.08	182.6	0.83	28.2	–	–	-	28.2	750.03	4.47	–
LC-CDs											
50	2. 38	134.8	0.84	53..41	0.58	0.73	2.1	55.5	381.43	3.55	49.2
100	1.68	128.2	0.87	64.41	7.78	0.53	2.7	67.11	315.01	2.87	58.0
150	2.09	125.9	0.83	78.6	0.09	0.71	3.2	81.26	260.02	1.97	65.3
200	1.88	90.78	0.89	291.0	2..3	0.61	12.2	303.2	69.87	0.98	90.7

inhibitors LC-CDs was around 0.25 Ω cm². However, the value increased after LC-CDs was added to the HCl environment, and the degree of the rise increased as the concentrations of LC-CDs increased. For LC-CDs, the greatest impedance value was 740 Ω cm² at 200 mg/l. These findings demonstrated that the inclusion of LC-CDs improved corrosion inhibition. Additionally, LC-CDs with a higher impedance value showed good corrosion inhibition.

For Bode phase angle chart in Figure 6d, when LC-CDs was added, the maximum phase angle increased, according to the Bode phase angle plot. The higher phase angle suggested a change toward more capacitive behavior and a slower corrosion process. Additionally, LC-CDs samples had a much greater phase angle and tended toward a pure capacitive nature. Furthermore, it indicated a single time constant related with the charge transfer mechanism, and in certain situations, a shrinking tail due to the relaxation process. Due to the longer cable connection between the working electrode and potentiostat, wire resistance may be the reason of the inductive behaviour noticed at the beginning of a few high frequencies with a phase angle below zero degrees.

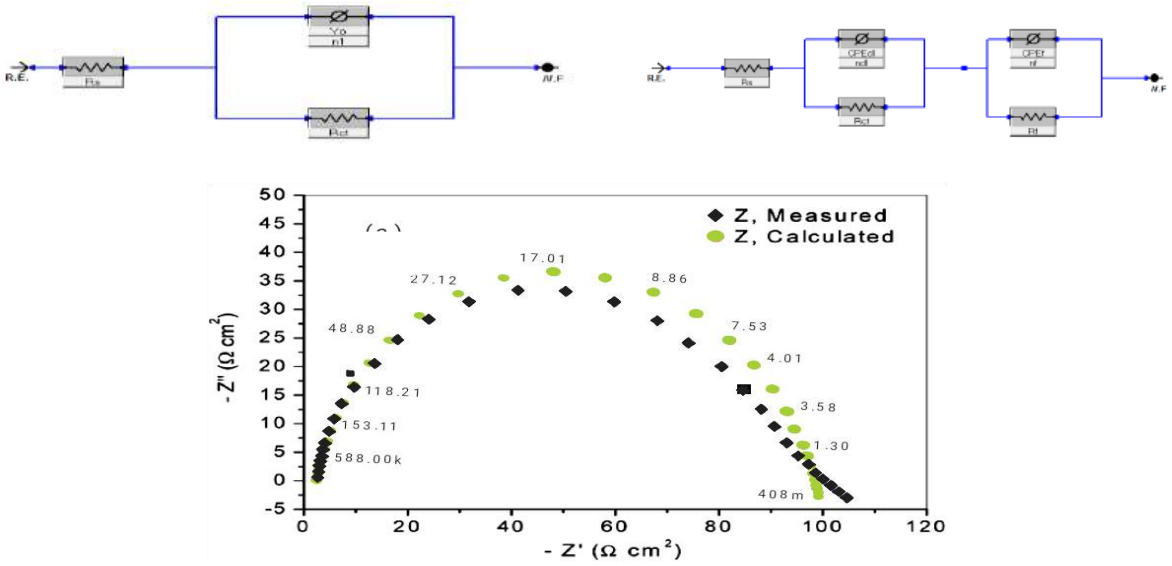

Figure 7. Equivalent circuit used to fit the experimental data for blank, and LC-CDs

Using the analogous circuit model, the Nyquist plot was fitted to have a better understanding of the different features of the EIS. The symbols R_{ct}, R_f, R_s, C_{dl}, and CPE stand for charge transfer resistance, film resistance, and solution resistance, double layer capacitance, and constant phase element respectively.

$$Z_{CPE} = Y_0^{-1}(j\omega)^{-ndl} \quad (4)$$

where

Y_0 = CPE constant

n_{dl} = CPE exponent;

j = $(-1)^{1/2}$ an imaginary number

ω = Angular frequency (rad/s)

Using the Equation 4, the double layer capacitance (C_{dl}), which is appropriate for non-ideal polarized electrodes where charge transfer governs the corrosion process, was calculated from the constant phase element's (CPE) solution resistance (Rs), charge transfer resistance (R_{ct}), exponent (n_{dl}), and proportionality factor (Y_{dl}):

$$C_{dl} = \sqrt[n_{dl}]{Y_o} \times \left(1/R_s + 1_{R_{ct}}\right)^{\left(1 - 1/n_{dl}\right)} \quad (5)$$

The electrochemical characteristics generated by the fittings are shown in Table 2. It is evident that the inclusion of the LC-CDs caused a significant rise in charge transfer resistance (R_{ct}), which was connected to the development of a surface layer. Additionally, the R_{ct} values rise as the concentration of LC-CDs increases, suggesting that more molecules are accessible for surface film formation at higher LC-CD concentrations. By shielding the steel surface from corrosive materials, the surface coating stops additional charge and mass transfer. Once more, R_{ct} values rise as C_{dl} values decrease, suggesting that the LC-CDs' adsorption increases the hydrophobicity of the steel surface. The polarization resistance (R_p) in the presence of LC-CDs is the sum of R_{ct}, R_f, and other resistances, such as accumulations at the metal/solution interface (Ra) and diffuse layer resistance (R_d) (Saigaa et al., 2023). Table 2 also shows the R_p values, which increase as the concentration of LC-CDs increases. At 200 mg/L, LC-CDs demonstrated exceptional performance with 90.7% efficiency. The observed decrease in C_{dl} values and the corresponding decline in Y_{dl} values indicated that the thickness of the adsorbed LC-CDs layer increased with an increase in LC-CDs concentration. Consequently, the higher concentration covered a large portion of the steel surface, deactivated the active sites, and considerably slowed down corrosion redox processes.

Table 3: Calculated values of f_a and f_c for the inhibition of LC-CDs

Inhibitor	Concentration (mg/l)	$-E_{corr}$(mV)	i_{corr} ($\mu A\ cm^{-2}$)	β_a ($mV\ dec^{-1}$)	$-\beta_c$ ($mV\ dec^{-1}$)	f_a	f_c	IE (%)
	Blank	-0.503	0.485	0.054	0,94	–	–	–
LC-CDs	50	-0.495	0.222	0.089	0.104	0.74	0.73	54.2
	100	-0.497	0.191	0.085	0.107	0.69	0.68	60.6
	150	-0.491	0.144	0.075	0.117	0.59	0.58	70.3
	200	-0.503	0.021	0.082	0.113	0.24	0.23	95.6

The computed values of f_a and f_c for the inhibition of LC-CDs, along with additional electrochemical parameters obtained via Tafel extrapolation, are shown in Table 3. Corrosion current densities were used to assess the effectiveness of LC-CDs as corrosion inhibitors. The values of f_a and f_c varied, and the E_{corr} displacement was noticeable for inhibition caused by reactive covering or the deactivation of active sites on the metal surface. When f_a and f_c are less than unity, the mechanism of inhibition is the deactivation of active sites. Inhibition occurs by reactive covering when either the value of f_a or f_c hits one, signifying acceleration in the oxidation half corrosion reaction or the reduction half corrosion reaction (Omran & Abdel-Salam, 2020). Table 3 makes it evident that f_a and f_c were not equal and that the values were less than one, indicating that the LC-CDs' deactivation of active sites stopped mild steel from corroding in a 1 M HCl solution. Furthermore, it is clear from Table 3 that the inclusion of LC-CDs considerably decreased Icorr, a measure of the rate of steel corrosion. The corrosion current density decreased most when 200 mg/l of LC-CDs were added. This was associated with a maximum inhibitory efficiency of 95.6% for LC-CDs. The corrosion potential increased to a higher positive value when LC-CDs were present compared to the blank. When evaluating steel's thermodynamic stability in acidic environments, the E_{corr} is an essential metric.

3.5 Potentiodynamic Polarization Measurements

PDP Tafel curves for mild steel in a 1 M HCl solution both with and without varying amounts of LC-CDs as seen in Figure 8. This figure makes it clear that, in comparison to the unrestrained steel sample, the presence of LC-CDs as corrosion inhibitors in corrosive solution caused the corrosion potential (E_{corr}) to modestly shift towards noble values (positive potential) as the concentration rose.

The difference in E_{corr} values of LC-CDs when added as inhibitor to the corrosive solution was less than ± 85 mV, as indicated in Table 3. This indicates that the inhibitor is mixed-type inhibitor that protect mild steel against corrosion in a 1 M HCl solution. This inhibitor prevent corrosion by delaying the generation of cathodic hydrogen and anodic dissolution (Mobin et al., 2022). LC-CDs was further verified to be mixed-type inhibitor because there were no notable displacements at the anodic (βa) or cathodic (βc) Tafel slopes.

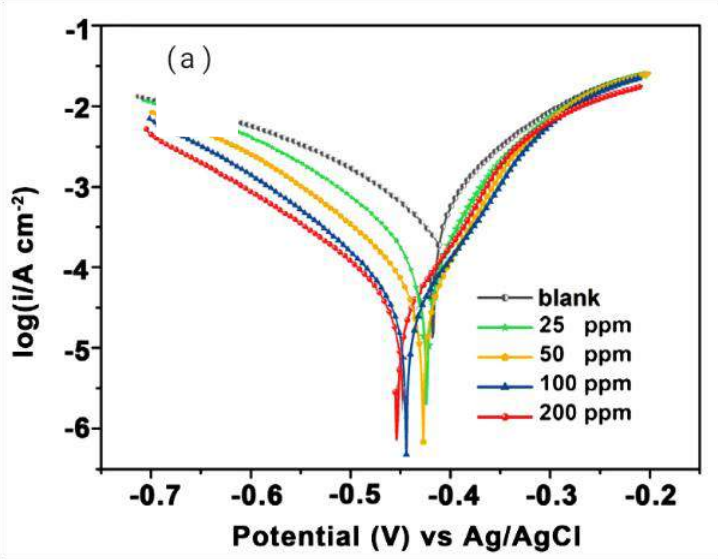

Figure 8. Potentiodynamic polarization curves for mild steel in 1 M HCl without and with different concentrations of LC-CDs at 25ºC

The mechanism of the corrosion response at the steel's anodic and cathodic sites remained unchanged by the presence of these inhibitors. LC-CDs and NLC-CDs prevented mild steel from corroding by obstructing the cathodic and anodic active sites. However, it might be said that the inhibition of anodic dissolution was more prevalent given the clear shifting of the anodic Tafel branch to more positive potential, as seen in Figure 8. This result is in line with the findings of Umoren et al., 2022, which states that the anodic and cathodic active areas on the steel surface are protected from corrosive species by introducing a carbon dots as an inhibitor into a corrosive solution (Umoren et al., 2022).

The presence of LC-CDs as corrosion inhibitor in the acid prevented corrosion by adsorbing their molecules on the steel's surface-active site to produce a protective layer that lowered the corrosion current densities. As shown in Table 3, the current densities (I_{corr}) values for the uninhibited sample dropped from 0.485 µA cm^2 to 0.021 µA cm^2 (LC-CDs) inhibited samples. This suggests that as inhibitor concentrations increased, less corrosion current passed through the samples. Using PDP experimental data and Equation 2, the corrosion inhibition efficiency of LC-CDs was evaluated, and the results as presented in Table 3 showed that their corrosion inhibition efficiency (IE) increased with increasing inhibitor concentration. The mild steel corrosion inhibited by LC-CDs had IE of 95.6, at an optimal inhibitor dose of 200 mg/l.

3.6 Surface Characterizations of Mild Steel Samples

SEM micrographs of the mild steel before and after 24 h of immersion in 1 M HCl solution in the absence and presence of 200 mg/L of LC-CDs. As observed in Figure 9, the contrast in the result showed obvious corrosion inhibition using LC-CDs as an inhibitor. Further surface characterization was carried out using Atomic Force Microscope to substantiate the efficiency of LC-CDs as potent corrosion inhibitor.

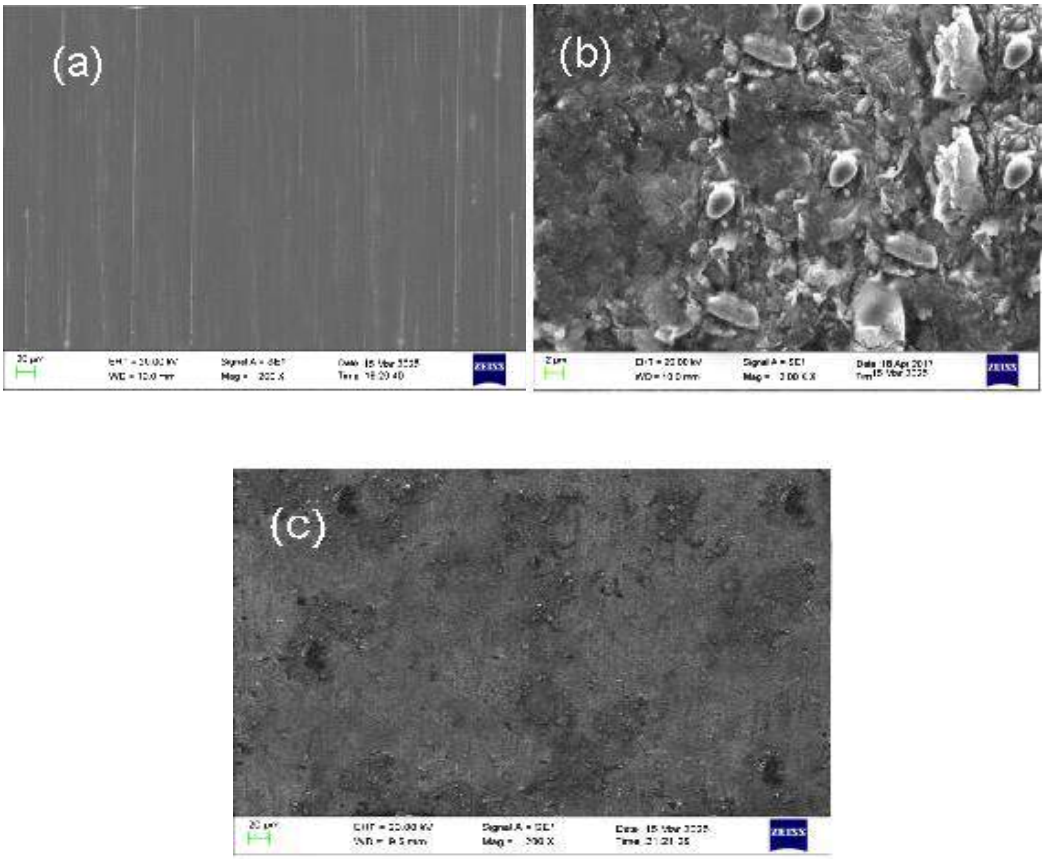

Figure 9. SEM Micrographs of (a) polished mild steel, (b) mild steel immersed in 1 M HCl solution, (c) mild steel immersed in 1 M HCl solution in the presence of 200 mg/L LC-CDs

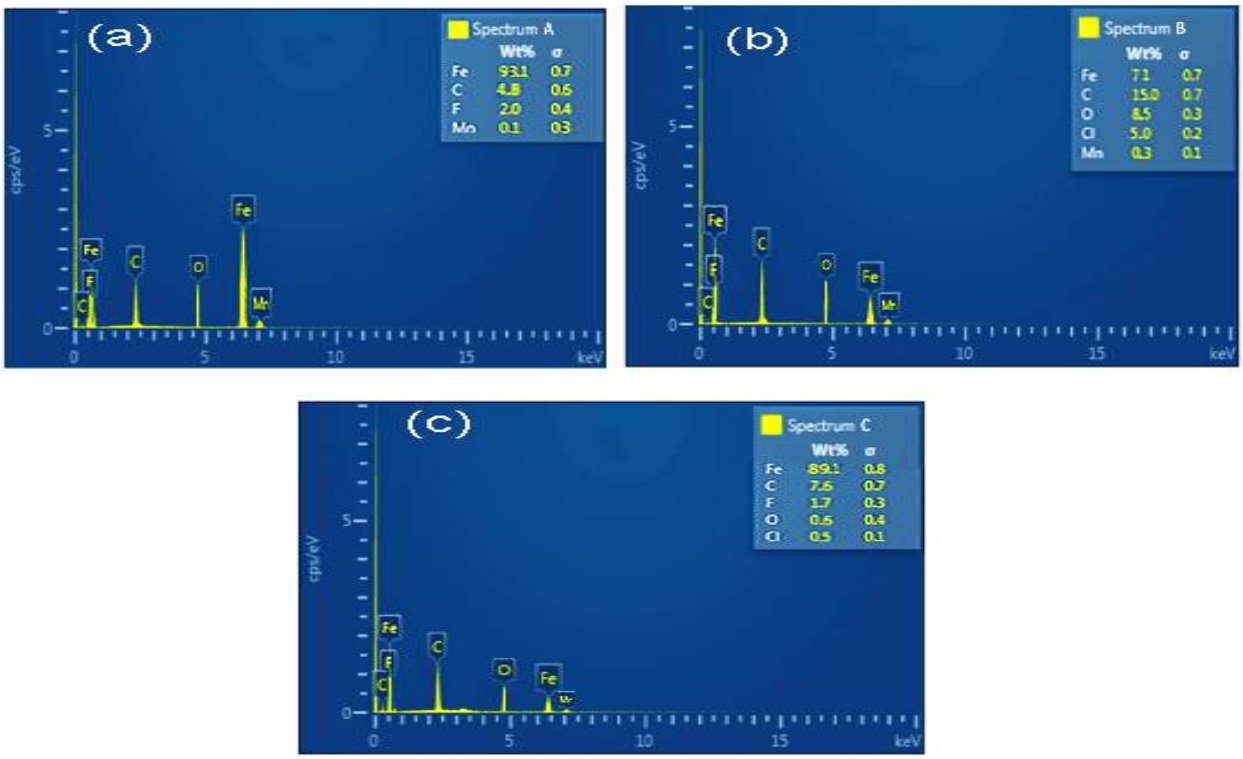

Figure: 10. EDS spectrum of (a) polished mild steel, (b) mild steel immersed in 1 M HCl solution, (c) mild steel immersed in 1 M HCl solution in the presence of 200 mg/L LC-CDs

Fig. 9a–c shows the SEM EDS pictures and the associated height profile of the mild steel before and after 24 hours of immersion in a 1 M HCl solution with and without 200 mg/L of LC-CDs. The SEM image of polished mild steel is shown in Figure 9a. With a surface roughness (Ra) of roughly 6.15 nm, the entire steel surface looked incredibly glossy and flat. The AFM 3D picture of mild steel submerged in a 1 M HCl blank solution is shown in Figure 9(b). The mild steel surface submerged in the blank solution clearly has more serious pits and pores than the polished surface in Figure 9a. The corresponding height profile of the surface shows a large surface roughness (Ra) of approximately 51.15 nm, indicating that the sample was severely corroded. The AFM 3D picture of polished mild steel submerged in a 1M HCl solution with LC-CDs is displayed in Figure 9c. As can be seen, the roughness parameters shown in Figure 9(c) are smaller than those in Figure 7(b), suggesting that the mild steel corrosion rate in 1M HCl solution was slowed down by the presence of LC-CDs. LC-CDs showed stronger corrosion-inhibiting properties and a lower surface roughness (Ra). The outcomes are in line with electrochemical and SEM findings.

After 24 hours in a corrosive solution, the surface of unfettered steel (Figure 9b) revealed a highly porous and severely damaged surface as a result of uniform corrosion attack by chloride and other corrosive species, which resulted in the development of porous flakes of iron corrosion products. Some of the elements were lost due to corrosion, according to the EDS corresponding to the samples (Figure 10b). For example, the Fe peak decreased to 80.6%, and among all the spectra, the chloride species, represented by the Cl atom, was present in the greatest quantity (4.6%). Additionally, an oxygen peak (8.3%) was found in this spectrum. These findings make it clear that the porous flakes (Figure 9b) were iron corrosion products created when chloride species attacked the steel (Subbiah et al., 2021).

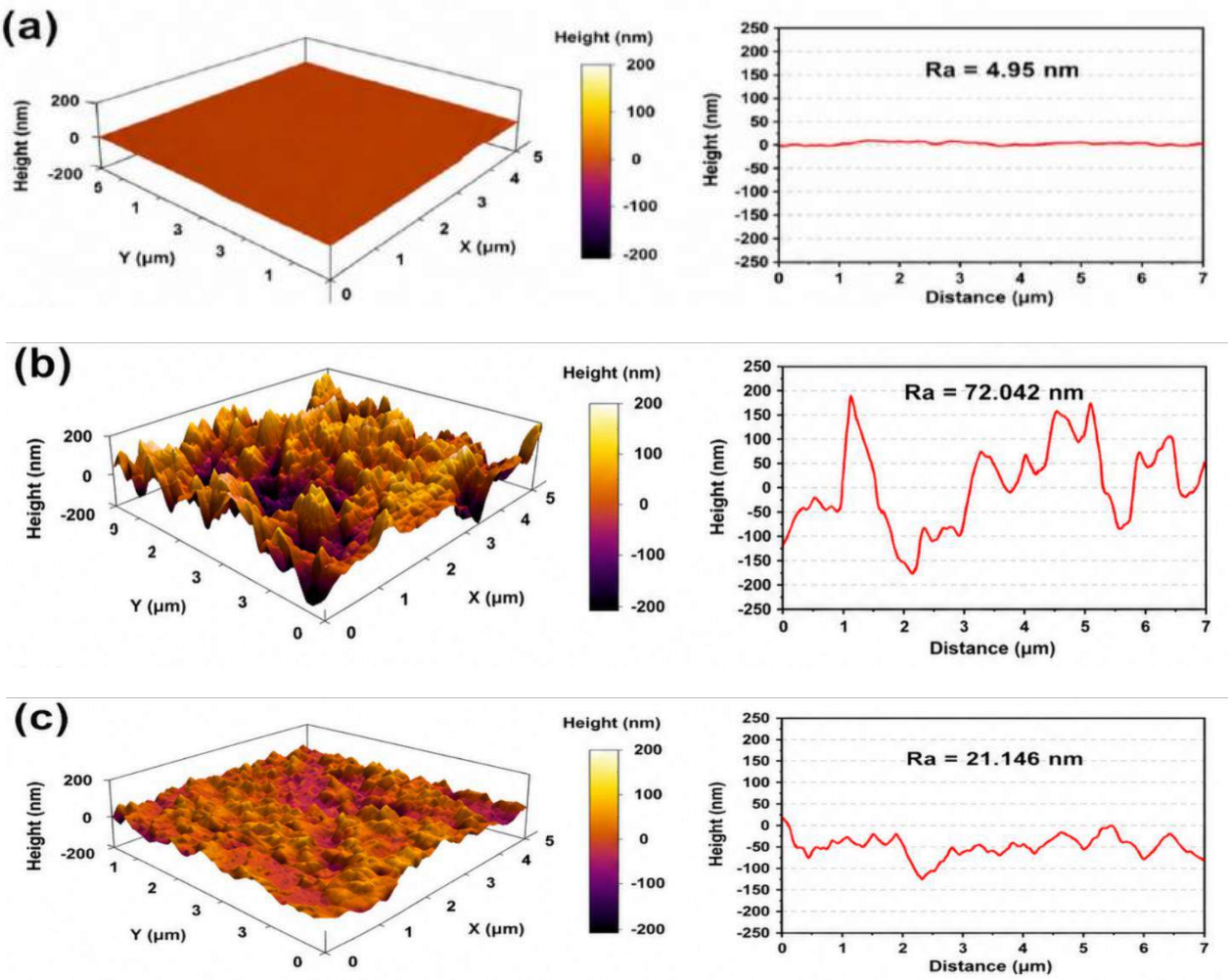

Figure 11. 2D and 3D AFM images of (a) polished mild steel, (b) mild steel immersed in 1 M HCl solution, (c) mild steel immersed in 1 M HCl solution in the presence of 200 mg/L LC-CDs 25^{0}C after 24 h.

The 2D and 3D Atomic Force Microscope (AFM) pictures of polished mild steel immersed in a 1M HCl solution at 30^{0}C for 24 hours with and without 200 mg/L lignin-containing cellulose-based carbon dots (LC-CDs) are shown in Figure 10. The AFM morphology of polished mild steel with a surface roughness (Ra) of around 13 nm is shown in Figure 11a, whereas the morphology of mild steel submerged in a 1M HCl blank solution is shown in Figure 11(b). Significant corrosion damage can be seen all over the mild steel surface. The mild steel surface's Ra value rose to 74.8 nm, as shown in Figure 11(b). However, when the mild steel was immersed in the acidic solution containing cellulose-based carbon dots (LC-CDs) that contained lignin, its roughness diminished. Compared to Figure 11(a), the roughness characteristics shown in Figure 11(c) are smaller. With a surface roughness value of roughly 54.0 for lignin-containing cellulose-based carbon dots (LC-CDs), the entire steel surface seemed incredibly smooth and glossy. These findings are consistent with findings from other applicable methods and imply that the substrate under study corroded less in the inhibited acid solution than in the blank acid solution.

4.0 Conclusion

This study investigated the potential of Lignin-Containing Cellulose derived carbon dots (LC-CDs) prepared from mature African fan palm (Borassus aethiopum) as corrosion inhibitor in 1M HCL. The successful creation of nanoscale carbonaceous materials appropriate for corrosion protection applications was confirmed by the hydrothermal conversion of pure cellulose, which resulted in well-dispersed, spherical carbon dots with an average particle size of roughly 5.38 nm.

UV and FTIR spectra were used to characterize the lignin-containing cellulose while TEM and SPM Morphologies were used to confirm that the inhibitor has been carbon doted to evident in its nano size and spherical shape.

Lignin-Containing Cellulose based carbon dots (LC-CDs) derived from prepared from mature African fan palm (Borassus aethiopum) exhibited high efficiency as green corrosion inhibitors for mild steel in 1 M HCl. Lignin-Containing Cellulose derived carbon dots (LC-CDs) had optimum IE of 90.8 when the optimal concentration of 200 mg/L was used from the gravimetric measurement. This was further analysed with EIS and PDP plots. The optimum inhibition efficiency of Lignin-Containing Cellulose based carbon dots (LC-CDs) was observed at 200 mg/L, and following a 48h immersion time. The higher values of IE at 60°C point to the chemisorption mode of adsorption of Lignin-Containing Cellulose based carbon dots (LC-CDs) molecules on the metal surface.

Surface observation of the uninhibited and inhibited steel samples using SEM/EDAX, 3D Surface profilometer images, and AFM confirmed that the Lignin-Containing Cellulose based carbon dots (LC-CDs) reduced the corrosive attack by forming a protective film on the steel surface leading to lessen surface roughness of the inhibited steel samples. Adsorption studies showed excellent performance of the synthesized carbon dot and its conformity to Langmuir adsorption isotherm indicating strong interaction between the inhibitor and the metal surface.

In all, Lignin-Containing Cellulose based carbon dots (LC-CDs) can serve as potential inhibitors for corrosion protection of mild steel during pickling, and descaling operations. The findings of the work showed that LC-CDs derived from *Borassus aethiopum* constitute a highly efficient, low cost, ecofriendly, and sustainable alternative to the conventional toxic corrosion inhibitors. Additionally, this study provides a future prospects in design and development of biomass derived carbon dots as next generation corrosion inhibitors

Acknowledgements

The authors are grateful for the support from the management and staff of the Polymer Engineering Department, Faculty of Engineering, Nnamdi Azikwe University, Awka.

Declaration of Generative AI and AI-assisted technologies in the writing process

During the preparation of this work the authors used ChatGPT in order to compare and analyse the mechanism of inhibition with related literatures in line with results obtained and further arranged the abstract already written. After using this tool, the authors reviewed and edited the content as needed and takes full responsibility for the content of the publication.

References

Abd-El-Nabey, B., El-Housseiny, S., Abd-El-Khalek, D., & Abd-El-Fatah, M. (2025). Ginger-derived carbon quantum dots as sustainable inhibitor of steel corrosion and barite precipitation. *Scientific Reports*, *15*(1), 25874.

Abraham, J. E., & Balachandran, M. (2022). Fluorescent mechanism in zero-dimensional carbon nanomaterials: a review. *Journal of Fluorescence*, *32*(3), 887-906.

Afolabi, O. J., Onen, A. I., Elabor, R., Akhabue, O. B., Oluwasegun, T., Madukwe, O., & Oyebanji, O. (2024). Adsorption characteristics of Luffa Cylindrica leaf extract as a corrosion inhibitor of copper in alkaline environment. *World J Adv Res Rev*, *23*(01), 3051-3082.

Ahmed, B., Mohammed, A., Kawady, N., Elaasy, I., & Soliman, E. (2024). Costly effective bioleaching of valuable metals from low grade ore using Aspergillus nidulans. *International Journal of Environmental Science and Technology*, *21*(6), 5469-5482.

Al-Amiery, A. A., Isahak, W. N. R. W., & Al-Azzawi, W. K. (2023). Corrosion inhibitors: natural and synthetic organic inhibitors. *Lubricants*, *11*(4), 174.

Al-Saadi, S., & Singh Raman, R. (2022). Silane coatings for corrosion and microbiologically influenced corrosion resistance of mild steel: a review. *Materials*, *15*(21), 7809.

Al Otaibi, N., & Hammud, H. H. (2021). Corrosion inhibition using harmal leaf extract as an eco-friendly corrosion inhibitor. *Molecules*, *26*(22), 7024.

Avdeev, Y. G., & Kuznetsov, Y. I. (2022). Acid corrosion of metals and its inhibition. A critical review of the current problem state. *International Journal of Corrosion and Scale Inhibition*, *11*(1), 111-141.

Bender, R., Féron, D., Mills, D., Ritter, S., Bäßler, R., Bettge, D., De Graeve, I., Dugstad, A., Grassini, S., & Hack, T. (2022). Corrosion challenges towards a sustainable society. *Materials and corrosion*, *73*(11), 1730 1751.

Cao, S., Zhao, Y., Cao, Y., Li, Y., Tan, H., & Wang, H. (2025). Ionic liquid-assisted biomass-derived N, S-doped carbon dots with enhanced corrosion inhibition. *Scientific Reports*, *15*(1), 23056.

Dave, P. N., & Macwan, P. M. (2024). Phytochemicals/Plant Extracts as Corrosion Inhibitors for Brass in Various Electrolytes. In *Phytochemistry in Corrosion Science* (pp. 296-328). CRC Press.

Dong, L., Wang, J., Ma, Y., Ruan, Y., Hu, Z., & Ma, X. (2024). Na-CDs as an eco-friendly and efficient corrosion inhibitor for Q235 in 1 M HCl. *Arabian Journal of Chemistry*, *17*(4), 105660.

Galo, G. T., Morandim-Giannetti, A. d. A., Cotting, F., Aoki, I. V., & Aquino, I. P. (2021). Evaluation of purple onion (Allium cepa L.) extract as a natural corrosion inhibitor for carbon steel in acidic media. *Metals and Materials International*, *27*(9), 3238-3249.

Gan, J., Chen, L., Chen, Z., Zhang, J., Yu, W., Huang, C., Wu, Y., & Zhang, K. (2023). Lignocellulosic biomass-based carbon dots: synthesis processes, properties, and applications. *Small*, *19*(48), 2304066.

Gitzhofer, F., Aluha, J., Langlois, P.-O., Barandehfard, F., Ntho, T. A., & Abatzoglou, N. (2021). Proven Anti-Wetting Properties of Molybdenum Tested for High-Temperature Corrosion-Resistance with Potential Application in the Aluminum Industry. *Materials*, *14*(18), 5355.

Holla, B. R., Mahesh, R., Manjunath, H., & Anjanapura, V. R. (2024). Plant extracts as green corrosion inhibitors for different kinds of steel: A review. *Heliyon*, *10*(14).

Hossain, N., Asaduzzaman Chowdhury, M., & Kchaou, M. (2021). An overview of green corrosion inhibitors for sustainable and environment friendly industrial development. *Journal of Adhesion Science and Technology*, *35*(7), 673-690.

Hui, S. (2023). Carbon dots (CDs): basics, recent potential biomedical applications, challenges, and future perspectives. *Journal of Nanoparticle Research*, *25*(4), 68.

Ituen, E., Singh, A., Yuanhua, L., & Li, R. (2020). Synthesis and evaluation of anticorrosion properties of onion mesocarp-nickel nanocomposites on X80 steel in acidic cleaning solution. *Journal of Materials Research and Technology*, *9*(3), 2832-2845.

Kaczmarek, A., Hoffman, J., Morgiel, J., Mościcki, T., Stobiński, L., Szymański, Z., & Małolepszy, A. (2021). Luminescent carbon dots synthesized by the laser ablation of graphite in polyethylenimine and ethylenediamine. *Materials*, *14*(4), 729.

Kadhim, A., Al-Amiery, A., Alazawi, R., Al-Ghezi, M., & Abass, R. (2021). Corrosion inhibitors. A review. *International Journal of Corrosion and Scale Inhibition*, *10*(1), 54-67.

Karim, M., Shokry, A., Ebrahim, S., & Khalil, M. (2022). The "ON-OFF" microwave reaction time technique: A novel strategy to impact the fluorescence of multi-color emissive carbon dots. *Colloids and Surfaces A: Physicochemical and Engineering Aspects*, *652*, 129735.

Kellal, R., Left, D. B., Azzi, M., & Zertoubi, M. (2023). Insight on the corrosion inhibition performance of Glebionis coronaria plant extract in various acidic mediums. *Journal of Applied Electrochemistry*, *53*(4), 811-832.

Kumar, V. B., Sahu, A. K., & Rao, K. B. S. (2022). Development of doped carbon quantum dot-based nanomaterials for lubricant additive applications. *Lubricants*, *10*(7), 144.

Kusumattaqiin, F., Pradana, B. A., & Halim, A. (2021). GELATIN AS A CORROSION BIOINHIBITOR AT SALINE MEDIA FROM FISH BONE OF MACKEREL (Scomberomorus sp). *Extraction*, *14*(3), 2177-2182.

Li, Y., Chen, Y., Wang, C., Li, Y., & Wu, Y. (2025). Exploring the potential of plant extracts as corrosion inhibitors: A comprehensive review. *Progress in Organic Coatings*, *198*, 108915.

Loachamin, D., Casierra, J., Calva, V., Palma-Cando, A., Ávila, E. E., & Ricaurte, M. (2024). Amine-based solvents and additives to improve the CO2 capture processes: a review. *ChemEngineering*, *8*(6), 129.

Mobin, M., Aslam, R., Salim, R., & Kaya, S. (2022). An investigation on the synthesis, characterization and anti-corrosion properties of choline based ionic liquids as novel and environmentally friendly inhibitors for mild steel corrosion in 5% HCl. *Journal of colloid and interface science*, *620*, 293-312.

MP, A., Pardhiya, S., & Rajamani, P. (2022). Carbon dots: an excellent fluorescent probe for contaminant sensing and remediation. *Small*, *18*(15), 2105579.

Nazibudin, N. A., Zainuddin, M. F., & Abdullah, C. C. (2023). Hydrothermal synthesis of carbon quantum dots: an updated review. *J. Adv. Res. Fluid Mech. Therm. Sci*, *101*(1), 192-206.

Omran, B. A., & Abdel-Salam, M. O. (2020). Basic corrosion fundamentals, aspects and currently applied strategies for corrosion mitigation. In *A New Era for Microbial Corrosion Mitigation Using Nanotechnology: Biocorrosion and Nanotechnology* (pp. 1-45). Springer.

Prakash, J., Kumar, P., Saxena, N., Pu, Z., Chen, Z., Tyagi, A., Zhang, G., & Sun, S. (2023). CdS based 3D nano/micro-architectures: formation mechanism, tailoring of visible light activities and emerging applications in photocatalytic H 2 production, CO 2 reduction and organic pollutant degradation. *Journal of Materials Chemistry A*, *11*(19), 10015-10064.

Ravi, S., Peters, S., Varathan, E., & Ravi, M. (2023). Molecular interaction and corrosion inhibition of benzophenone and its derivative on mild steel in 1 N HCl: electrochemical, DFT and MD simulation studies. *Colloids and Surfaces A: Physicochemical and Engineering Aspects*, *661*, 130919.

Saigaa, N., Bouguessa, S., Boukhedena, W., Nacer, M., Nadji, A., & Gouasmia, A. (2023). Optimization of the inhibition corrosion of carbon steel in an acidic medium by a novel eco-friendly inhibitor Asphodelus ramosus using response surface methodology. *Journal of Electrochemical Science and Engineering*, *13*(3), 469-490.

Shahmoradi, A., Talebibahmanbigloo, N., Nickhil, C., Nisha, R., Javidparvar, A., Ghahremani, P., Bahlakeh, G., & Ramezanzadeh, B. (2022). Molecular-MD/atomic-DFT theoretical and experimental studies on the

quince seed extract corrosion inhibition performance on the acidic-solution attack of mild-steel. *Journal of Molecular Liquids*, *346*, 117921.

Shekhar, C., Jaiswal, A., Ji, G., & Prakash, R. (2021). Ethanol extract of waste potato peels for corrosion inhibition of low carbon steel in chloride medium. *Materials today: proceedings*, *44*, 2267-2272.

Subbiah, K., Lee, H.-S., Mandal, S., & Park, T. (2021). Conifer cone (Pinus resinosa) as a green corrosion inhibitor for steel rebar in chloride-contaminated synthetic concrete pore solutions. *ACS applied materials & interfaces*, *13*(36), 43676-43695.

Tang, Z., Huang, W., Liu, L., Li, H., Meng, H., Zeng, T., Ye, X., Jiang, Q., Ye, Y., & Liu, Y. (2024). Study on structure and molecular scale protection mechanism of green Ce, N-CDs anti-bacterial and anti-corrosive inhibitor. *Journal of Materials Research and Technology*, *28*, 3865-3881.

Ul Haq, I., Qasim, A., Lal, B., Zaini, D. B., Foo, K. S., Mubashir, M., Khoo, K. S., Vo, D.-V. N., Leroy, E., & Show, P. L. (2022). Ionic liquids for the inhibition of gas hydrates. A review. *Environmental Chemistry Letters*, *20*(3), 2165-2188.

Umoren, P. S., Kavaz, D., & Umoren, S. A. (2022). Corrosion inhibition evaluation of chitosan–CuO nanocomposite for carbon steel in 5% HCl solution and effect of KI addition. *Sustainability*, *14*(13), 7981.

Usman, A.-L. (2025). Eco-Friendly Synthesis of Silver Nanoparticles from African Fan Palm (Borassus aethiopum) Leaf Extract for Corrosion Inhibition of Mild Steel in 1 M HCl: A Weight Loss Analysis. *Journal of Science Innovation and Technology Research*.

Vaidya, N. R., Aklujkar, P., & Rao, A. R. (2022). Modification of natural gums for application as corrosion inhibitor: a review. *Journal of Coatings Technology and Research*, *19*(1), 223-239.

Vashi, R. (2025). Natural honey as eco-friendly corrosion inhibitor for metals and alloys-a review. *Port Electrochim Acta*, *43*, 365-375.

Verma, C., Ebenso, E. E., Quraishi, M., & Hussain, C. M. (2021). Recent developments in sustainable corrosion inhibitors: design, performance and industrial scale applications. *Materials Advances*, *2*(12), 3806-3850.

Wang, X., Chen, L., Yang, F., Xiang, Q., & Liu, J. (2023). Corrosion inhibition mechanism and extraction technology of plant corrosion inhibitors: a review. *Journal of Adhesion Science and Technology*, *37*(21), 2919-2943.

Xu, Z., Gan, Y., Zeng, J., Chen, J., Fu, A., Zheng, X., & Li, W. (2023). Green synthesis of functionalized fluorescent carbon dots from biomass and their corrosion inhibition mechanism for copper in sulfuric acid environment. *Chemical Engineering Journal*, *470*, 144425.

Yadav, S., & Daniel, S. (2024). Green synthesis of zero-dimensional carbon nanostructures in energy storage applications—a review. *Energy Storage*, *6*(1), e500.

Yang, Z., Xu, T., Li, H., She, M., Chen, J., Wang, Z., Zhang, S., & Li, J. (2023). Zero-dimensional carbon nanomaterials for fluorescent sensing and imaging. *Chemical Reviews*, *123*(18), 11047-11136.

Zehra, S., Mobin, M., Parveen, M., & Ahmad, R. (2025). Corrosion Fundamentals: Understanding the Science Behind the Damage. *Industrial Corrosion: Fundamentals, Failure, Analysis and Prevention*, 1-16.